PHOTONICS Research

High-power passively Q-switched 2 μm all-solid-state laser based on a Bi_2Te_3 saturable absorber

X. Liu,[1] K. Yang,[1,2,3,*] S. Zhao,[1] T. Li,[1] W. Qiao,[1] H. Zhang,[2] B. Zhang,[2] J. He,[2] J. Bian,[3] L. Zheng,[4] L. Su,[4] and J. Xu[5]

[1]School of Information Science and Engineering, and Shandong Provincial Key Laboratory of Laser Technology and Application, Shandong University, Jinan 250100, China
[2]State Key Laboratory of Crystal Material, Shandong University, Jinan 250100, China
[3]State Key Laboratory of Pulsed Power Laser Technology, Hefei 230031, China
[4]Key Laboratory of Transparent and Opto-functional Inorganic Materials, Artificial Crystal Research Center, Shanghai Institute of Ceramics, Chinese Academy of Sciences, Shanghai 201899, China
[5]School of Physics Science and Engineering, Institute for Advanced Study, Tongji University, Shanghai 200092, China
*Corresponding author: k.j.yang@sdu.edu.cn

Received 13 July 2017; revised 8 August 2017; accepted 8 August 2017; posted 11 August 2017 (Doc. ID 302430); published 6 September 2017

By using the ultrasound-assisted liquid phase exfoliation method, Bi_2Te_3 nanosheets are synthesized and deposited onto a quartz plate to form a kind of saturable absorber (SA), in which nonlinear absorption properties around 2 μm are analyzed with a home-made mode-locked laser. With the as-prepared Bi_2Te_3 SA employed, a stable passively *Q*-switched all-solid-state 2 μm laser is successfully realized. *Q*-switched pulses with a maximum average output power of 2.03 W are generated under an output coupling of 5%, corresponding to the maximum single-pulse energy of 18.4 μJ and peak power of 23 W. The delivered shortest pulse duration and maximum repetition rate are 620 ns and 118 kHz under an output coupling of 2%, respectively. It is the first presentation of such Bi_2Te_3 SA employed in a solid-state *Q*-switched crystalline laser at 2 μm, to the best of our knowledge. In comparison with other 2D materials suitable for pulsed 2 μm lasers, the saturable absorption performance of Bi_2Te_3 SA is proved to be promising in generating high power and high-repetition-rate 2 μm laser pulses.

OCIS codes: (140.3070) Infrared and far-infrared lasers; (140.3580) Lasers, solid-state; (140.3540) Lasers, Q-switched; (160.4330) Nonlinear optical materials; (160.4236) Nanomaterials.

https://doi.org/10.1364/PRJ.5.000461

1. INTRODUCTION

Benefitting from the nature of strong absorption by water as well as eye safety, 2 μm lasers have a series of applications in various fields, such as laser surgery, free-space communication, and coherent LIDAR [1–3] and have gained much attention. Especially, the pulsed laser deposition [4] and pumping sources for optical parametric oscillations [3] to generate mid-infrared radiations demand pulsed lasers with high power. *Q*-switching is a direct way to generate such pulsed laser sources. The crucial optical components for *Q*-switches include active modulators such as acoustic and electro-optical modulation module and passive modulators such as different saturable absorbers (SAs). Compared with active *Q*-switching, passive *Q*-switching based on SA is advantageous in compactness, convenience, and low-cost. Exploring novel SAs with high quality and performance, especially those suitable for the mid-infrared lasers developed quickly in recent years, is always a hot topic. Before 2003, the commonly used SA for pulsed lasers was a semiconductor saturable absorber mirror (SESAM), which, however, was soon substituted by low-cost and easily synthetized carbon nanotubes (CNTs) due to the complicated fabrication process and necessary expensive facilities. Since then, different structured CNTs have been widely investigated in both *Q*-switching and mode-locking lasers [5,6]. Since 2004, when the single-layer carbon atom was successfully exfoliated from graphite, 2D graphene has become the most attractive SA in generating laser pulses with high performance [7–9]. Although graphene has intrinsic advantages of broadband absorption, controllable modulation depth, and low nonsaturable loss, the relatively low modulation depth and low damage threshold prohibit the generation of high pulse energy and high-power pulsed lasers [10].

Similar to the Dirac electronic structure of graphene, which is known as a Dirac cone [11], another group of 2D materials, topological insulators (TIs), has been proposed and investigated in recent years. Generally, bulk TIs materials have a small

bandgap, but a gapless metallic surface state is generated in layered 2D TIs, which are caused by strong spin-orbit coupling and time-reversal symmetry [12]. With such typical band structure, 2D TIs materials show broadband absorption like CNTs and graphene and have become promising optical modulators candidates in generating laser pulses. In 2012, the saturable absorption property of TIs was first demonstrated at 1.5 μm by Bernard *et al.* [13]. Since then, a lot of research on TI materials has sprung up in a wide spectral range covering 1–3 μm. For fiber lasers, using either bulk or layered TIs as SAs, both *Q*-switching and mode-locking operations have been realized, from which short and even ultrashort laser pulses have been obtained with pulse durations ranging from several hundred of femtoseconds to several microseconds [14–16]. Nevertheless, the inherent undesirable nonlinear effects in fiber limit the *Q*-switched laser performance at ~2 μm. As demonstrated in Refs. [15,16], the Bi_2Te_3 SA *Q*-switched fiber lasers could only generate ~2 μm pulses with durations wider than 1.7 μs, repetition rates lower than 60 kHz, output powers below 30 mW and the pulse energies smaller than 1 μJ. As for solid-state lasers, pulsed operations based on TI SAs have been achieved in Nd^{3+}, Yb^{3+}, Er^{3+}, and Pr^{3+} ion-doped bulk lasers [17–22] around 1, 1.6, and 604 nm, respectively. Very recently, Jiang *et al.* employed a few-layered Bi_2Te_3 SA in a Tm:ZBLAN waveguide laser and realized *Q*-switched mode-locking operation [23]. However, the obtained maximum output power was as low as 16.3 mW at a corresponding maximum repetition rate of 44.1 kHz, and the achieved shortest pulse duration was as large as 1.4 μs; thus, the pulse generation ability of Bi_2Te_3 SA needs to be further explored. Furthermore, benefitting from the high thermal conductivity and energy storage ability, crystalline lasers can provide a suitable environment and margin for the employment of novel SA. Thus, incorporating the Bi_2Te_3 SA in a solid-state laser, the pulsed laser characteristics, including high output power, short pulse duration, and large repetition rate, are highly expected to be improved.

In this paper, we successfully synthesized a kind of Bi_2Te_3 SA on a quartz plate and characterized its nonlinear absorption properties at 2 μm. By using the as-fabricated Bi_2Te_3 SA in a diode-pumped solid-state Tm:LuAG laser, passive *Q*-switching laser operation was realized at 2023 nm, and the output laser performance, including the average output power, pulse duration, and repetition rates, as recorded and analyzed. A maximum output power of 2.03 W has been achieved, corresponding to the maximum single pulse energy of 18.4 μJ and peak power of 23 W under an output coupling of 5%. The shortest pulse duration of 620 ns was obtained at a maximum repetition rate of 118 kHz under an output coupling of 2%. The temporal profiles of the pulse train and the shortest pulse as well as the emission spectrum also were recorded and presented at the end of this paper.

2. PREPARATION AND CHARACTERIZATION OF Bi_2Te_3 SA

The synthesis of Bi_2Te_3 nanosheets were performed by using the UALPE method, which has been widely used due to its low cost and convenience. The raw Bi_2Te_3 powder, with a purity of 99.99% and size of around 5 μm, was bought from a commercial company, in which 678 mg Bi_2Te_3 powder and 10 mL absolute ethyl alcohol were mixed in centrifuge tube. Then the centrifuge tube was sonicated in an ultrasonic machine for 12 h with a power of 100 W. After the sonication process, Bi_2Te_3 nanosheets were formed and floated in the alcohol, along with the residual bulk Bi_2Te_3. To divide the nanosheets from the bulk Bi_2Te_3, the centrifuge tube was kept standing in a beaker for 10 h. Finally, 10 μL suspension was absorbed by a suction pipet from the two-thirds resultant mixture suspension and dripped onto a quartz plate with a size of 20 mm × 20 mm × 0.5 mm. Soon, the mixture solution on the substrate was dried, and a Bi_2Te_3 SA was well prepared.

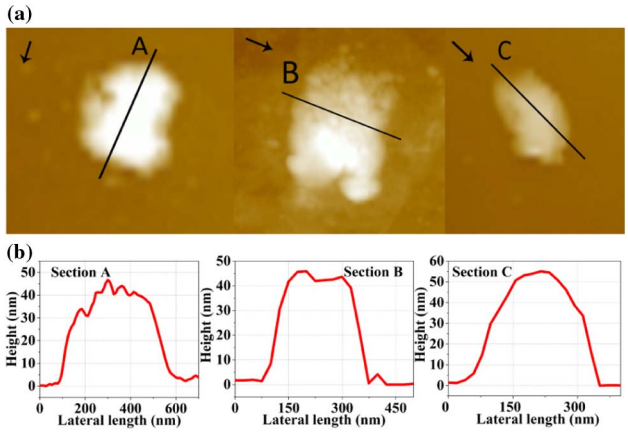

Fig. 1. (a) Surface topography of three typical Bi_2Te_3 nanosheets. (b) Height profiles of selected nanosheets.

To characterize the quality of as-prepared Bi_2Te_3 SA, the surface topography was measured by atomic force microscopy (AFM), as shown in Fig. 1(a). Three typical nanosheets were selected and analyzed. The height profiles of the selected three nanosheets were recorded along the black line, as shown in Fig. 1(a), and three symbols of arrowhead on the top corner showed the measurement direction of height profiles. As can be seen in Fig. 1(b), the as-prepared Bi_2Te_3 nanosheets had thicknesses of ~50 nm, which was the key factor to determine the modulation depth and the unsaturable loss of Bi_2Te_3 SA, and the widths of Bi_2Te_3 nanosheets were around 400 nm, which were much smaller than the original Bi_2Te_3 powder, confirming the excellent ultrasonic peeling under the power of 100 W and duration of 12 h and the availability of peeling solvent of absolute ethyl alcohol.

The nanostructured Bi_2Te_3 SA was further identified using a Raman spectrometer (LabRAM HR800) with a resolution of 1.29 cm^{-1} and excitation wavelength of 633 nm. To compare the difference of Raman response between bulk and layered Bi_2Te_3, the powdered Bi_2Te_3 and synthesized Bi_2Te_3 SA were measured, respectively. The optical phonon peaks for bulk Bi_2Te_3 were observed to locate at ~41, ~62.73 , ~102.87, and ~135.25 cm^{-1}, corresponding to the vibration modes of E_g^1, A_{1g}^1, E_g^2, and A_{1g}^2, respectively. In comparison with the bulk Bi_2Te_3 sample, the synthesized Bi_2Te_3 nanosheets showed an additional peak of 118.41 cm^{-1} marked in Fig. 2, which was related to the unique vibration mode (A_{1u}^2) for exfoliated Bi_2Te_3, coming from the breaking of crystalline symmetry originating from the ~400 nm width of Bi_2Te_3 nanosheets [24,25].

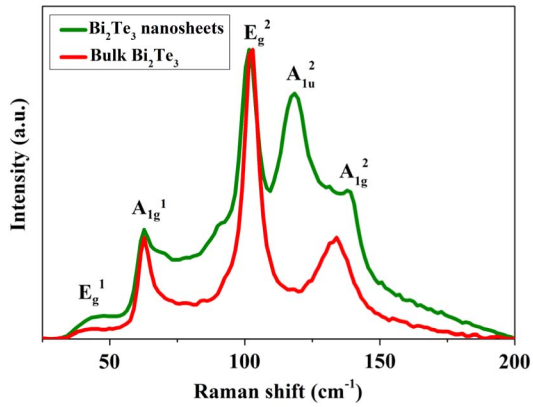

Fig. 2. Measured Raman spectrum of bulk Bi_2Te_3 and Bi_2Te_3 nanosheets.

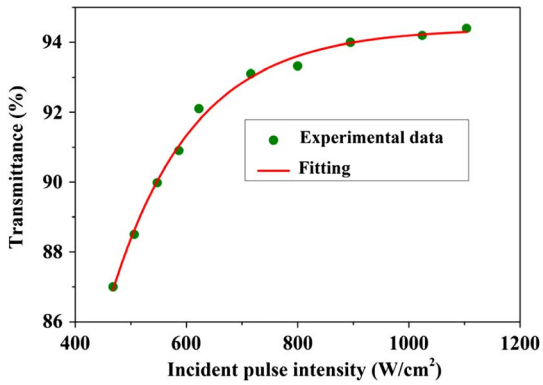

Fig. 3. Nonlinear optical properties of the as-prepared Bi_2Te_3 SA.

One of the most important properties for a SA is its nonlinear optical response. With a home-made mode-locked 2 μm laser employed, which emitted a pulse with duration of 40 ps and wavelength of 2009 nm, the nonlinear absorption property of Bi_2Te_3 SA was investigated (see Fig. 3). The modulation depth, nonsaturable loss and saturation intensity were estimated 7.5%, 5.5%, and 786 W/cm^2, respectively. Figure 4 shows the optical transmission of the Bi_2Te_3 nanosheets dripped on a quartz plate. The transmission at 2 μm was measured to be 88.3%. Considering the Bi_2Te_3 has a bandgap of ~0.2 eV, the transmission of longer wavelength can be seen in Ref. [26].

3. LASER EXPERIMENT AND RESULTS

To further characterize the saturable absorption property of the as-prepared Bi_2Te_3 SA under laser operation, a simple plano–concave cavity was employed (the schematic setup is shown in Fig. 5). The physical length of the whole laser cavity was 2.5 cm. A fiber-coupled diode laser with a maximum output power of 50 W and output wavelength of 787 nm was employed as the pump source. Through a 1:1 imaging module, the pump light was focused into the laser crystal with a beam radius of 200 μm. M_1 was a concave dichroic mirror with a curvature radius of 200 mm and employed as

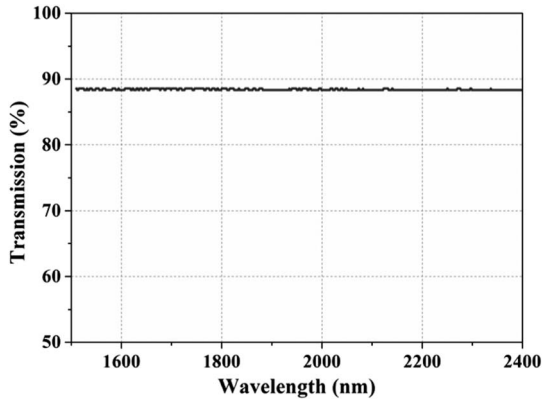

Fig. 4. Optical transmission spectrum of Bi_2Te_3 nanosheets.

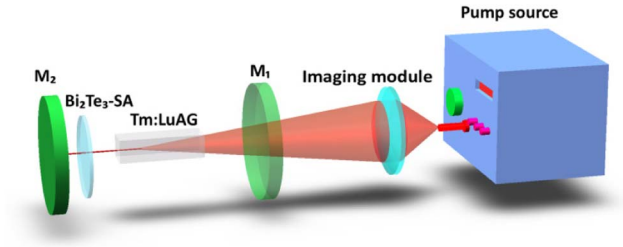

Fig. 5. Schematic setup of diode-pumped Bi_2Te_3 Q-switched Tm:LuAG laser.

an input mirror, which was anti-reflectivity (AR) coated from 750 to 850 nm (reflectivity < 2%) and high reflectivity (HR) coated (reflectivity > 99.9%) from 1850 to 2100 nm. A Tm:LuAG crystal with 6 at.% Tm^{3+} ions doping and a size of 4 mm × 4 mm × 8 mm was used as the gain medium, both faces of which were AR coated from 750 to 850 nm (reflectivity < 2%) and 1830–2230 nm (reflectivity < 0.8%). To efficiently remove the accumulated heat, the laser crystal was wrapped by indium foil and embedded in a brass heat sink, which was water cooled at 14°C. M_2 was a flat mirror and worked as an output coupler (OC). For comparisons of laser performance, two OCs with different transmittances of 2% and 5% were utilized. The Bi_2Te_3 SA was placed near the OC M_2 as close as possible to obtain large power intensity.

The average output powers were measured by a laser power meter (MAX 500AD, Coherent, USA). First, the CW Tm:LuAG laser characteristics were recorded; Fig. 6(a) shows that the maximum output powers for OCs of $T = 2\%$ and $T = 5\%$ were 1.9 and 2.16 W, respectively, corresponding to slope efficiencies of 17% and 20%. Figure 6(b) shows the average output power performance of a diode-pumped Bi_2Te_3 SA Q-switched Tm:LuAG laser. Using two OCs with different transmittances of 2% and 5%, two sets of average output powers were recorded and plotted, shown as dots in Fig. 6(b). When the incident pump power exceeded 0.8 and 1.2 W for $T = 2\%$ and $T = 5\%$ OCs, respectively, the laser began to oscillate and directly ran into Q-switching operation. With the incident pump powers increased from 2 to 12 W, the

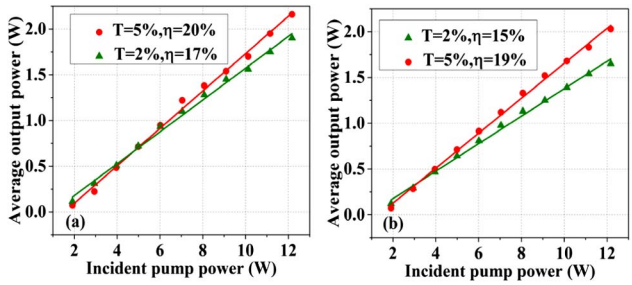

Fig. 6. Average output powers versus incident pump powers for the Bi_2Te_3 SA Q-switched Tm:LuAG laser (a) in CW regime and (b) Q-switching regime.

average output powers increased almost linearly for both $T = 2\%$ and $T = 5\%$ OCs. As shown in Fig. 6(b), the dependence of average output powers on incident pump powers was linearly fitted, and a slope efficiency of 19% was obtained for the $T = 5\%$ OC, which was higher than that of 15% for the case of $T = 2\%$ OC. Under Q-switching operation, a maximum average output power of 2.03 W was achieved for the $T = 5\%$ OC, which was also higher than that of 1.65 W for the case of $T = 2\%$ OC. In the experiment, the as-prepared Bi_2Te_3 SA sample was found to be easily damaged when the incident pump power exceeded 12 W, corresponding to an intracavity peak power intensity of about 2.7 MW/cm^2 on the Bi_2Te_3 SA, which was regarded as the damage threshold of the as-prepared Bi_2Te_3 SA. The relatively low damage threshold was attributed to the unwanted impurities introduced into the Bi_2Te_3 SA during the imperfect fabrication process [27]. To protect the laser crystal and Bi_2Te_3 SA from being damaged, the incident pump power was not increased beyond 12 W. Additionally, using a laser spectrometer (APE WaveScan, APE Inc.) with a resolution of 0.4 nm, the emission spectra from the Tm:LuAG laser with and without the Bi_2Te_3 SA were recorded and shown in Fig. 7, respectively. As shown in Fig. 7, without the Bi_2Te_3 SA in the cavity, the output wavelength was centered at 2027 nm with an FWHM of 15 nm, while the center wavelength blueshifted to 2023.6 nm with an FWHM of 3 nm when the Bi_2Te_3 SA was inside the cavity. The change of output spectra was attributed to the insertion loss induced

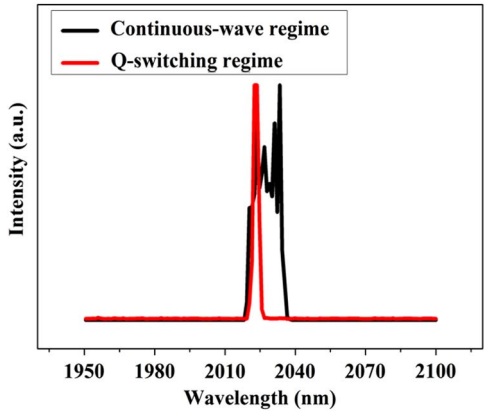

Fig. 7. Output spectra for Tm:LuAG lasers in CW regime and Q-switching regime.

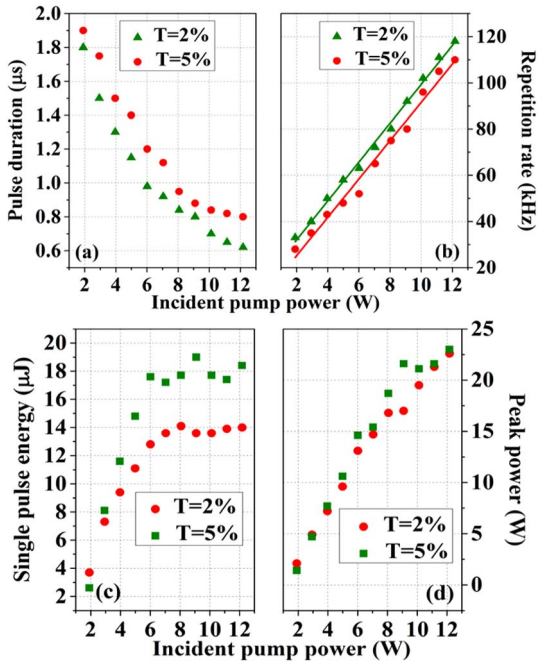

Fig. 8. (a) Pulse durations, (b) repetition rates, (c) single pulse energies, and (d) peak powers as function of incident pump powers.

by the Bi_2Te_3 SA, which not only increased the inversion rate in a typical three-level laser system leading to a spectral blueshift but narrowed the spectrum because the low-gain laser modes were prevented from oscillating.

The output pulse characteristics were detected by a fast InGaAs photodetector (EOT, ET-5000, USA) with a response time of 35 ps and monitored by a digital oscilloscope (1 GHz bandwidth, Tektronix DPO 7102, USA). The dependences of pulse duration, repetition rate, single pulse energy, and peak power on incident pump powers are summarized in Fig. 8. From Fig. 8(a), the pulse duration shows nearly linear decline tendency for both cases of $T = 2\%$ and 5% OCs when the incident pump power was below 9 W; however, the pulse durations tended to decrease slowly with the further augmentation of incident pump powers for both cases. We attributed this phenomenon to the decrease of ground state population of Tm^{3+} ions due to the high-intensity pumping. Under the maximum incident pump power of 12 W, the shortest pulse durations for $T = 2\%$ and 5% OCs were 620 and 800 ns, respectively. The relationship between the pulse repetition rates and incident pump powers is shown Fig. 8(b), from which we can see that the repetition rate almost linearly increased with the augmentation of the incident pump power, and no saturation tendency was observed for both cases of $T = 2\%$ and 5% OCs. Within the pump power range in the experiment, the repetition rates ranged from 33 to 118 kHz and 28 to 110 kHz for $T = 2\%$ and 5% OCs, respectively. Figures 8(c) and 8(d) show the variations of single pulse energies and peak powers against incident pump powers. Initially, the single pulse energies augmented steadily with the increase of incident pump powers. At the incident pump power of about 6 W, the increase trend ceased and the single pulse energy became

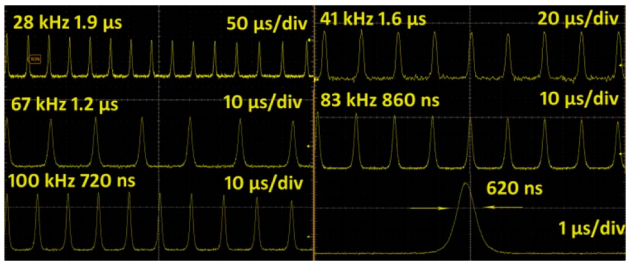

Fig. 9. Temporal profiles of typical pulse trains at different repetition rates and the shortest pulse shape with duration of 620 ns.

somehow saturated, probably due to the thermal effect happening to the laser crystal and Bi_2Te_3 SA. As seen in Fig. 8(c), maximum single pulse energies of 14 and 18.4 μJ were obtained, respectively, for the $T = 2\%$ and 5% OCs. Figure 8(d) presents the dependence of peak powers on the incident pump powers, which are calculated by using single-pulse energies and pulse durations. It can be seen that the delivered pulse peak powers varied from 2.1 to 22.6 W and 1.4 to 23 W for the cases of $T = 2\%$ and 5% OCs, respectively, and no apparent saturation tendency was found in both cases. The temporal pulse profiles were recorded, as shown in Fig. 9. The typical pulse trains at different repetition rates of 28, 41, 67, 83, and 100 kHz were summarized for comparisons, from which a maximum pulse-to-pulse instability of 3.5% was observed, showing a good Q-switching stability. The temporal profile of the shortest pulse with duration of 620 ns was also recorded, as shown in Fig. 9. By using a 90.0/10.0 scanning-knife-edge method, the M^2 factors of the Q-switched laser beam under the maximum output power were measured to be 1.62 and 1.59 in the tangential and sagittal planes, respectively, as shown in Fig. 10.

It should be noticed that the obtained pulse laser characteristics, including a maximum average output power of 2.03 W under the output coupling of 5%, corresponding to a maximum single pulse energy of 18.4 μJ and peak power of 23 W as well as a minimum pulse duration of 620 ns at a maximum repetition rate of 118 kHz under the output coupling of 2% were all superior to those from the Bi_2Te_3 SA Q-switched fiber lasers, as shown in Refs. [15,16]. Furthermore, compared

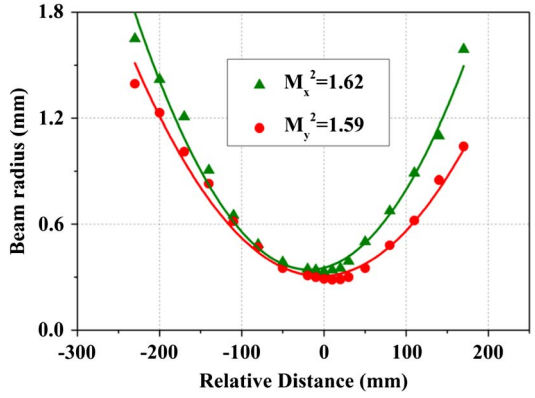

Fig. 10. M^2 factors from the Bi_2Te_3 SA Q-switched Tm:LuAG laser at the highest output power.

with other 2D material-based SA, including graphene, WS_2, MoS_2, and black phosphorus (BP), the single-pulse energy we obtained here is only smaller to that generated by BP SA at 2 μm wavelength [28–31]. But the insurmountable disadvantage of easy oxidation of BP limits the application of BP-based SA. In summary, the achieved pulse characteristics well indicated the excellent performance of as-prepared Bi_2Te_3 SA in generating stable solid-state 2 μm laser pulses with high power and high repetition rate. From this point of view, Bi_2Te_3 SA can act as a promising modulator candidate to generate a high pulse energy laser.

4. CONCLUSION

In this paper, a kind of Bi_2Te_3 SA has been fabricated by UALPE method, and the nonlinear optical properties have been characterized. With the as-prepared SA, an all-solid-state passively Q-switched 2 μm laser was successfully achieved. It was the first demonstration of Bi_2Te_3 SA utilized in realizing a crystalline pulsed laser at 2 μm, to the best of our knowledge. The obtained shortest pulse duration was 620 ns at a maximum repetition rate of 118 kHz under an output coupling of $T = 2\%$. A maximum average output power of 2.03 W was delivered from the realized Bi_2Te_3 SA-based Q-switched laser, corresponding to the maximum single pulse energy of 18.4 μJ and peak power of 23 W under an output coupling of $T = 5\%$, respectively. The experimental results indicated the promising potential of Bi_2Te_3 in generating mid-infrared laser pulses with high power and high pulse energy.

Funding. National Natural Science Foundation of China (NSFC) (61475088, 61775119, 61378022, 61422511); Young Scholars Program of Shandong University (2015WLJH38); Open Research Fund of the State Key Laboratory of Pulsed Power Laser Technology, Electronic Engineering Institute, Hefei, China (SLK2016KF01).

REFERENCES

1. N. M. Fried and K. E. Murray, "High-power thulium fiber laser ablation of urinary tissues at 1.94 μm," J. Endourol. **19**, 25–31 (2005).
2. S. W. Henderson, P. J. M. Suni, C. P. Hale, S. M. Hannon, J. R. Magee, D. L. Bruns, and E. H. Yuen, "Coherent laser radar at 2 μm using solid-state lasers," IEEE Trans. Geosci. Remote Sens. **31**, 4–15 (1993).
3. K. Scholle, S. Lamrini, P. Koopmann, and P. Fuhrberg, "2 μm laser sources and their possible applications," in *Frontiers in Guided Wave Optics and Optoelectronics* (Intech, 2010), pp. 471–500.
4. G. I. Petrov, V. V. Yakovlev, and N. I. Minkovski, "High-energy short-pulse diode-pumped Nd: YVO_4 laser and its applications for material sciences and biomedical imaging," in *IEEE Conference on Lasers and Electro-Optics (CLEO)* (2003), p. 2.
5. A. Y. Chamorovskiy, A. V. Marakulin, A. S. Kurkov, T. Leinonen, and O. G. Okhotnikov, "High-repetition-rate Q-switched holmium fiber laser," IEEE Photon. J. **4**, 679–683 (2012).
6. M. Jung, J. Koo, Y. M. Chang, P. Debnath, Y.-W. Song, and J. H. Lee, "An all fiberized, 1.89-μm Q-switched laser employing carbon nanotube evanescent field interaction," Laser Phys. Lett. **9**, 669–673 (2012).
7. Q. Bao, H. Zhang, Y. Wang, Z. Ni, Y. Yan, Z. X. Shen, K. P. Loh, and D. Y. Tang, "Atomic-layer graphene as a saturable absorber for ultrafast pulsed lasers," Adv. Funct. Mater. **19**, 3077–3083 (2009).
8. Y. M. Chang, H. Kim, J. H. Lee, and Y.-W. Song, "Multilayered graphene efficiently formed by mechanical exfoliation for nonlinear

saturable absorbers in fiber mode-locked lasers," Appl. Phys. Lett. **97**, 211102 (2010).
9. J.-L. Xu, X.-L. Li, Y.-Z. Wu, X.-P. Hao, J.-L. He, and K.-J. Yang, "Graphene saturable absorber mirror for ultra-fast-pulse solid-state laser," Opt. Lett. **36**, 1948–1950 (2011).
10. Y.-Y. Lin, P. Lee, J.-L. Xu, C.-L. Wu, C.-M. Chou, C.-Y. Tu, M. M. C. Chou, and C.-K. Lee, "High-pulse-energy topological insulator Bi2Te3 based passive Q-switched solid-state laser," IEEE Photon. J. **8**, 1–10 (2016).
11. J. E. Moore, "The birth of topological insulators," Nature **464**, 194–198 (2010).
12. J. Lee, M. Jung, J. Koo, C. Chi, and J. H. Lee, "Passively Q-switched 1.89-μm fiber laser using a bulk-structured Bi_2Te_3 topological insulator," IEEE J. Sel. Top. Quantum Electron. **21**, 264–269 (2015).
13. F. Bernard, H. Zhang, S. Gorza, and P. Emplit, "Towards mode-locked fiber laser using topological insulators," in *Advanced Photonics Congress*, OSA Technical Digest (Optical Society of America, 2012), paper NTh1A.5.
14. J. Lee, J. Koo, Y. M. Jhon, and J. H. Lee, "A femtosecond pulse erbium fiber laser incorporating a saturable absorber based on bulk-structured Bi_2Te_3 topological insulator," Opt. Express **22**, 6165–6173 (2014).
15. J. Lee, J. Koo, and J. H. Lee, "Thulium-Holmium-codoped, passively Q-switched fiber laser incorporating Bi2Te3 saturable absorber," in *Asia Communications and Photonics Conference*, C. Lu, J. Luo, Y. Ji, K. Kitayama, H. Tam, K. Xu, P. Ghiggino, and N. Wada, eds., OSA Technical Digest (Optical Society of America, 2015), paper AM2C.4.
16. N. H. M. Apandi, F. Ahmad, S. N. F. Zuikafly, M. H. Ibrahim, and S. W. Harun, "Bismuth (III) telluride (Bi2Te3) embedded in PVA as a passive saturable absorber in a 2 micron region," Photon. Lett. Poland **8**, 101–103 (2016).
17. H. Yu, H. Zhang, Y. Wang, C. Zhao, B. Wang, S. Wen, H. Zhang, and J. Wang, "Topological insulator as an optical modulator for pulsed solid-state lasers," Laser Photon. Rev. **7**, L77–L83 (2013).
18. B. Wang, H. Yu, H. Zhang, C. Zhao, S. Wen, H. Zhang, and J. Wang, "Topological insulator simultaneously Q-switched dual-wavelength Nd:Lu_2O_3 laser," IEEE Photon. J. **6**, 1–7 (2014).
19. F. Lou, R. Zhao, J. He, Z. Jia, X. Su, Z. Wang, J. Hou, and B. Zhang, "Nanosecond-pulsed, dual-wavelength, passively Q-switched ytterbium-doped bulk laser based on few-layer MoS_2 saturable absorber," Photon. Res. **3**, A25–A29 (2015).
20. Y.-J. Sun, C.-K. Lee, J.-L. Xu, Z.-J. Zhu, Y.-Q. Wang, S.-F. Gao, H.-P. Xia, Z.-Y. You, and C.-Y. Tu, "Passively Q-switched tri-wavelength Yb^{3+}:GdAl3(BO3)4 solid-state laser with topological insulator Bi_2Te_3 as saturable absorber," Photon. Res. **3**, A97–A101 (2015).
21. B. Huang, P. Tang, J. Yi, G. Jiang, J. Liu, Y. Zou, C. Zhao, and S. Wen, "Resonantly pumped Er: YAG laser Q-switched by topological insulator nanosheets at 1617 nm," Opt. Mater. (2016) (online).
22. Y. Cheng, J. Peng, B. Xu, H. Xu, Z. Cai, and J. Weng, "Passive Q-switching of Pr: LiYF 4 orange laser at 604 nm using topological insulators Bi_2Se_3 as saturable absorber," Opt. Laser Technol. **88**, 275–279 (2017).
23. X. Jiang, S. Gross, H. Zhang, Z. Guo, M. J. Withford, and A. Fuerbach, "Bismuth telluride topological insulator nanosheet saturable absorbers for q-switched mode-locked Tm: ZBLAN waveguide lasers," Annalen der Physik **528**, 543–550 (2016).
24. C. Chi, J. Lee, J. Koo, and H. J. Lee, "All-normal-dispersion dissipative-soliton fiber laser at 1.06 μm using a bulk-structured Bi_2Te_3 topological insulator-deposited side-polished fiber," Laser Phys. **24**, 105106 (2014).
25. Y.-H. Lin, S.-F. Lin, Y.-C. Chi, C.-L. Wu, C.-H. Cheng, W.-H. Tseng, J.-H. He, C.-I. Wu, C.-K. Lee, and G.-R. Lin, "Using n-and p-type Bi_2Te_3 topological insulator nanoparticles to enable controlled femtosecond mode-locking of fiber lasers," ACS Photon. **2**, 481–490 (2015).
26. J. Li, H. Luo, L. Wang, C. Zhao, H. Zhang, H. Li, and Y. Liu, "3-μm mid-infrared pulse generation using topological insulator as the saturable absorber," Opt. Lett. **40**, 3659–3662 (2015).
27. P. Li, G. Zhang, H. Zhang, C. Zhao, J. Chi, Z. Zhao, C. Yang, H. Hu, and Y. Yao, "Q-switched mode-locked Nd:YVO_4 laser by topological insulator Bi_2Te_3 saturable absorber," IEEE Photon. Technol. Lett. **26**, 1912–1915 (2014).
28. J. Hou, B. Zhang, J. He, Z. Wang, F. Lou, J. Ning, R. Zhao, and X. Su, "Passively Q-switched 2 μm Tm:YAP laser based on graphene saturable absorber mirror," Appl. Opt. **53**, 4968–4971 (2014).
29. C. Luan, K. Yang, J. Zhao, S. Zhao, L. Song, T. Li, H. Chu, J. Qiao, C. Wang, Z. Li, S. Jiang, B. Man, and L. Zheng, "WS2 as a saturable absorber for Q-switched 2 micron lasers," Opt. Lett. **41**, 3783–3786 (2016).
30. L. C. Kong, G. Q. Xie, P. Yuan, L. J. Qian, S. X. Wang, H. H. Yu, and H. J. Zhang, "Passive Q-switching and Q-switched mode-locking operations of 2 μm Tm:CLNGG laser with MoS2saturable absorber mirror," Photon. Res. **3**, A47–A50 (2015).
31. H. Zhang, J. He, Z. Wang, J. Hou, B. Zhang, R. Zhao, K. Han, K. Yang, H. Nie, and X. Sun, "Dual-wavelength, passively Q-switched Tm:YAP laser with black phosphorus saturable absorber," Opt. Mater. Express **6**, 2328–2335 (2016).